ARTICLE

Check for updates

Quantum and nonlinear effects in light transmitted through planar atomic arrays

Robert J. Bettles[1,2], Mark D. Lee[3], Simon A. Gardiner[1] & Janne Ruostekoski [4✉]

Understanding strong cooperative optical responses in dense and cold atomic ensembles is vital for fundamental science and emerging quantum technologies. Methodologies for characterizing light-induced quantum effects in such systems, however, are still lacking. Here we unambiguously identify significant quantum many-body effects, robust to position fluctuations and strong dipole–dipole interactions, in light scattered from planar atomic ensembles by comparing full quantum simulations with a semiclassical model neglecting quantum fluctuations. We find pronounced quantum effects at high atomic densities, light close to saturation intensity, and around subradiant resonances. Such conditions also maximize spin–spin correlations and entanglement between atoms, revealing the microscopic origin of light-induced quantum effects. In several regimes of interest, our approximate model reproduces light transmission remarkably well, permitting analysis of otherwise numerically inaccessible large ensembles, in which we observe many-body analogues of resonance power broadening, vacuum Rabi splitting, and significant suppression in cooperative reflection from atomic arrays.

[1] Joint Quantum Center (JQC) Durham–Newcastle, Department of Physics, Durham University, Durham DH1 3LE, UK. [2] ICFO-Institut de Ciencies Fotoniques, The Barcelona Institute of Science and Technology, 08860 Castelldefels (Barcelona), Spain. [3] Insight Risk Consulting, 16–18 Monument Street, Prospect Business Centres, London EC3R 8AJ, UK. [4] Physics Department, Lancaster University, Lancaster LA1 4YB, UK. ✉email: j.ruostekoski@lancaster.ac.uk

Light can mediate strong interactions between atoms, inducing strong position-dependent correlations, even in the limit of low light intensity, when the response (for the case of a simple level structure) is entirely classical. Such a correlated optical response can differ dramatically from that predicted by standard electrodynamics of continuous media, where resonant-light-induced dipole–dipole (DD) interactions between atoms are treated in an averaged sense[1,2]. Beyond the limit of low light intensity, an isolated atom can scatter light quantum-mechanically (such as in the incoherent Mollow spectrum[3]), and quantum effects in the interactions of light with dilute atomic ensembles have been utilized in, e.g., quantum information protocols[4]. In strongly interacting dense systems the possible role of quantum and cooperative effects is less clear and has been the subject of long-standing debate[1,5–8]. A particularly promising system to explore and utilize strong light-induced DD interactions is a regular planar array of scatterers, such as atoms. As shown both theoretically and experimentally, in the linear low-excitation limit these manifest a wealth of phenomena, e.g., subdiffraction features[9,10], nontrivial topological phases[11,12], transmission varying from complete reflection to full transparency[13–19], narrow resonances, and subradiance[15–17,20–27], as well as quantum technological applications[28,29] and other collective effects[30–35].

We show that we can identify quantum effects in the light transmitted through planar arrays and uniform-density disks of cold and dense atomic ensembles. Many-body quantum correlations are induced by light-atom coupling, which, surprisingly, survive even strong many-body resonant DD interactions and atomic position fluctuations. Specifically, comparing the correlated optical response determined using the quantum master equation (QME) to simulations neglecting any quantum fluctuations between atomic levels in different atoms [referred to as the "semiclassical" equations (SCEs)[36]], we systematically identify light-established quantum effects between atoms in the transmitted light as a function of atom confinement, density, and driving intensity. The effect of many-body quantum fluctuations on the scattering manifests most prominently at high densities when the light is close to saturation intensity, and especially significantly in the vicinity of subradiant resonances. We find that these conditions also produce maximal spin–spin correlations and entanglement of formation in the underlying atomic system, further confirming the role of many-body quantum correlations and entanglement in observing a difference in light transmission between QME and SCEs models. Incorporating the single-atom quantum description of light emission into the semiclassical scattering, we can typically use SCEs also for incoherent scattering to qualitatively reproduce the full quantum scattering even in the regimes where quantum effects in coherent scattering are most pronounced, and elsewhere also quantitatively. SCEs therefore allow us to analyze cooperative transmission of light through large atomic arrays and disks beyond the limit of low light intensity, without needing to solve the full strongly-interacting quantum dynamics. Doing so, we find collective phenomena due to DD interactions that are many-body analogs of power broadening and vacuum Rabi splitting of atomic resonances in cavities[37,38], and demonstrate a significant effect of intensity on the transmission that may ultimately restrict the utilization of atomic arrays as highly reflective cooperative mirrors.

Results

An appealing feature of light scattering from cold atoms[39–50] is that light-mediated strong DD interactions can establish correlations between atoms at fluctuating positions, which are most simply described using atomic field operators for the ground and excited states $\hat{\psi}_{g,e}(\mathbf{r})$. Hence, $\langle \hat{\mathbf{P}}^+(\mathbf{r}) \rangle = \langle \hat{\psi}_g^\dagger(\mathbf{r}) \mathbf{d}_{ge} \hat{\psi}_e(\mathbf{r}) \rangle$ denotes
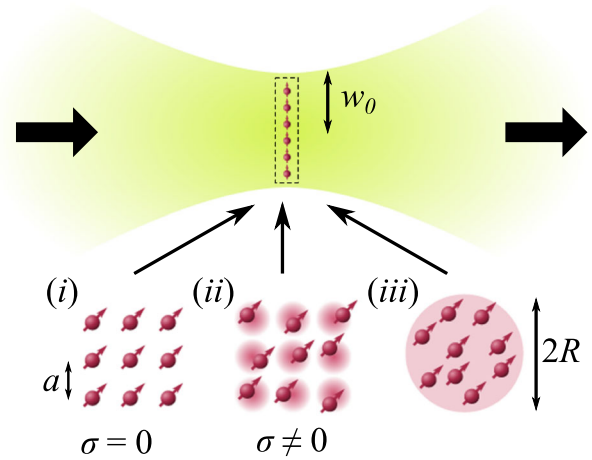

Fig. 1 Schematic illustration. A laser beam (waist w_0) focused onto an ensemble of atoms arranged in: (*i*) a planar square array with interatomic spacing a; (*ii*) as in (*i*) but with standard deviation σ normally-distributed fluctuations around their mean positions; (*iii*) random positions within a radius R uniform-density thin disk.

the positive frequency component of the light-induced atomic polarization, where $\mathbf{d}_{ge} = \mathbf{d}_{eg}^*$ is the dipole matrix element, and the populations are $\langle \hat{\psi}_g^\dagger(\mathbf{r}) \hat{\psi}_g(\mathbf{r}) \rangle$ and $\langle \hat{\psi}_e^\dagger(\mathbf{r}) \hat{\psi}_e(\mathbf{r}) \rangle$. Because of the DD interactions, the polarization and populations also depend on two-body correlations $\langle \hat{\psi}_a^\dagger(\mathbf{r}) \hat{\psi}_b^\dagger(\mathbf{r}') \hat{\psi}_c(\mathbf{r}') \hat{\psi}_d(\mathbf{r}) \rangle$, where $a, b, c, d \in \{g, e\}$, representing the correlations in the optical response of an atom at $\mathbf{r}$ given the presence of a second atom at $\mathbf{r}'$. These in turn depend on three-body correlations, etc., resulting in a hierarchy of equations of motion for correlation functions[51,52]. In a cold, dense ensemble (Fig. 1) this hierarchy can significantly and nonperturbatively modify the scattering behavior even in the classical regime, invalidating attempts to truncate it[1]. This is a key ingredient in, e.g., Anderson localization of light, which has been a subject of considerable controversy and debate[53,54].

Quantum master equation. A numerical device for solving this correlation function hierarchy is to treat the atoms as discrete point particles, meaning for a particular configuration of atomic positions $\{\mathbf{r}_1, ..., \mathbf{r}_N\}$ that two-body correlation functions take the form

$$\left\langle \hat{\psi}_a^\dagger(\mathbf{r}) \hat{\psi}_b^\dagger(\mathbf{r}') \hat{\psi}_c(\mathbf{r}') \hat{\psi}_d(\mathbf{r}) \right\rangle_{\{\mathbf{r}_1, ..., \mathbf{r}_N\}}$$
$$= \sum_{j\ell(j\neq\ell)} \rho_{ad;bc}^{(j,\ell)} \delta(\mathbf{r} - \mathbf{r}_j) \delta(\mathbf{r}' - \mathbf{r}_\ell), \tag{1}$$

where $\rho_{ad;bc}^{(j,\ell)}$ denote correlation functions of the internal atomic energy levels only[36]. We then solve the internal atom dynamics at discrete positions, and the new correlation functions simply emerge from the N-body density matrix $\rho \equiv \rho_{\{\mathbf{r}_1, ..., \mathbf{r}_N\}}$. This evolves according to QME:

$$\dot{\rho} = -\frac{i}{\hbar} \left[\sum_j H_{\mathrm{sys},j} - \sum_{j\ell(j\neq\ell)} \hbar\Omega_{j\ell} \hat{\sigma}_+^{(j)} \hat{\sigma}_-^{(\ell)}, \rho \right]$$
$$+ \sum_{j\ell} \gamma_{j\ell} \left(2\hat{\sigma}_-^{(j)} \rho \, \hat{\sigma}_+^{(\ell)} - \hat{\sigma}_+^{(\ell)} \hat{\sigma}_-^{(j)} \rho - \rho \hat{\sigma}_+^{(\ell)} \hat{\sigma}_-^{(j)} \right), \tag{2}$$

where the collective scattering is represented by the dispersive $\Omega_{j\ell}$ and dissipative $\gamma_{j\ell}$ DD interactions, the single-atom half-width at half-maximum (HWHM) linewidth by $\gamma_{jj} = \gamma$, and $\hat{\sigma}_+^{(j)} = (\hat{\sigma}_-^{(j)})^\dagger = |e\rangle_{jj}\langle g|$. For simplicity, we consider two-level

atoms and the Hamiltonian

$$H_{\text{sys},j} = -\hbar\Delta\hat{\sigma}_{ee}^{(j)} - \mathbf{d}_{eg} \cdot \boldsymbol{\mathcal{E}}^+(\mathbf{r}_j)\hat{\sigma}_+^{(j)} - \mathbf{d}_{ge} \cdot \boldsymbol{\mathcal{E}}^-(\mathbf{r}_j)\hat{\sigma}_-^{(j)}, \quad (3)$$

where $\boldsymbol{\mathcal{E}}^+ = (\boldsymbol{\mathcal{E}}^-)^*$ is the positive-frequency-component of the frequency $\omega = kc = 2\pi c/\lambda$ laser field, detuned from the atomic resonance frequency ω_{ge} by $\Delta = \omega - \omega_{ge}$ and $\hat{\sigma}_{ee}^{(j)} = |e\rangle_{jj}\langle e|$. We take the polarization of the incident field to be parallel to the orientation of the atomic dipoles. Spatial correlations are numerically synthesized by ensemble-averaging over stochastic realizations of atomic positions sampled from the density distribution[36,55]. Solving Eq. (2) for large systems is numerically taxing, although few-atom ensembles already demonstrate many-body effects in their spectra[56].

Semiclassical model. In the limit of low light intensity, where the excited state population vanishes, the internal level correlations, such as those described by $\rho_{\text{ad};bc}^{(j,\ell)}$ in Eq. (1), also vanish for two-level atoms. The stochastic electrodynamics simulations are then formally exact[36,55], reproducing the many-atom spatial correlations, which are identical to those occurring in the classical electrodynamics of coupled linear electric dipoles. Beyond the limit of low light intensity, the full dynamics of Eq. (2) can be greatly simplified by factorizing the internal atomic level correlation functions:

$$\rho_{\text{ad};bc}^{(j,\ell)} \simeq \rho_{\text{ad}}^{(j)}\rho_{bc}^{(\ell)}. \quad (4)$$

Following the formalism of ref. [36] we then obtain coupled nonlinear equations:

$$\frac{d}{dt}\rho_{ge}^{(j)} = (i\Delta - \gamma)\rho_{ge}^{(j)} - \frac{i}{\hbar}\left(2\rho_{ee}^{(j)} - 1\right)\mathbf{d}_{eg} \cdot \boldsymbol{\mathcal{E}}^+(\mathbf{r}_j)$$
$$- i\left(2\rho_{ee}^{(j)} - 1\right)\sum_{\ell \neq j}\left(\Omega_{j\ell} + i\gamma_{j\ell}\right)\rho_{ge}^{(\ell)}, \quad (5)$$

$$\frac{d}{dt}\rho_{ee}^{(j)} = -2\gamma\,\rho_{ee}^{(j)} + \frac{2}{\hbar}\text{Im}\left[\boldsymbol{\mathcal{E}}^-(\mathbf{r}_j) \cdot \mathbf{d}_{ge}\,\rho_{ge}^{(j)}\right]$$
$$+ 2\,\text{Im}\left[\sum_{\ell \neq j}\rho_{ge}^{(j)}\left(\Omega_{j\ell} - i\gamma_{j\ell}\right)\rho_{ge}^{(\ell)*}\right]. \quad (6)$$

Note the relatively small number of equations $2N$ compared to the full quantum system size 2^N. This formalism has been applied to the modeling of pumping of atoms in dense clouds[50], and has also been extended to cavity quantum electrodynamics (QED)[57].

Spatially correlated scattering between different atoms is accounted for in Eqs. (5) and (6) via $\Omega_{j\ell}$ and $\gamma_{j\ell}$ (for $\Omega_{j\neq\ell} = \gamma_{j\neq\ell} = 0$ they reduce to the independent-atom optical Bloch equations). In the limit of low light intensity the ensemble-averaged response of SCEs coincides with the exact classical electrodynamics; beyond this limit, the model incorporates nonlinear internal level dynamics of the atoms. However, because of the factorization in Eq. (4), they cannot account for many-body quantum entanglement between different atoms' internal levels. Finding situations in which the predictions of SCEs observably differ from the full QME solution therefore identifies light-induced quantum effects in the transmitted light. Conversely, regimes where quantum fluctuations are minimal allow for the simulation of much larger systems than are accessible with QME, and also test the validity of related approaches in other contexts, based, e.g., on mean-field approximations, intensity expansions, or truncations of the correlations[58–62].

Light-established quantum effects in transmitted light. We begin by calculating the coherent (Fig. 2a–c) and incoherent (Fig. 2d–f) forward transmission, T_{coh} and T_{inc} (see "Methods"

section), through planar square arrays and thin disks of $N = 4$ atoms (Fig. 1), and the corresponding relative differences (Fig. 3a–c) between quantum and semiclassical results (for the effects of a larger 3×3 array, see Supplementary Note 1). The array could be realized, e.g., by an optical lattice[63] or dipole traps[64,65]. Unless otherwise stated, we consider lattice spacing $a = 0.25\lambda$ and disk radius $R = 0.28\lambda$. Physically, we calculate the far-field light intensity in the same mode as the driving field $\boldsymbol{\mathcal{E}}^\pm(\mathbf{r})$, integrated over the polar angle $\sin\theta \lesssim 0.24$ (see "Methods" section and Supplementary Note 2). We account for the fluctuations in atomic positions due to finite trap confinement by ensemble-averaging over many stochastic realizations of position configurations (see "Methods" section)[10]. Light-induced position-dependent correlations between the atoms (see earlier "hierarchy of correlation functions") exist also classically, since the DD interactions depend on the precise interatomic separations. These classical many-body position correlations are therefore present in both the full quantum $T_{\text{coh}}^{\text{QM}}$ and semiclassical $T_{\text{coh}}^{\text{SC}}$ transmissions, but all quantum effects have been neglected in $T_{\text{coh}}^{\text{SC}}$. Hence, we unambiguously identify quantum effects in the coherent transmission by the difference $T_{\text{coh}}^{\text{QM}} - T_{\text{coh}}^{\text{SC}}$. Moreover, since the coherent scattering for a single atom is always purely classical, $T_{\text{coh}}^{\text{QM}} - T_{\text{coh}}^{\text{SC}}$ cannot depend on the single-atom response, and therefore represents quantum correlations solely due to many-body effects.

To obtain the incoherently scattered light $\langle\delta\hat{\mathbf{E}}_d^-(\mathbf{r})\,\delta\hat{\mathbf{E}}_d^+(\mathbf{r})\rangle$, we write the scattered light field as $\hat{\mathbf{E}}_d^+ = \langle\hat{\mathbf{E}}_d^+\rangle + \delta\hat{\mathbf{E}}_d^+$, where $\delta\hat{\mathbf{E}}_d^+$ denotes the fluctuations[66]. This yields the incoherent transmission (see "Methods" section), from which we also isolate quantum behavior by $T_{\text{inc}}^{\text{QM}} - T_{\text{inc}}^{\text{SC}}$, in which case all the quantum effects have again been systematically neglected in $T_{\text{inc}}^{\text{SC}}$. Although the coherent scattering of a single atom is classical, this is not the case for the incoherent emission. We can improve the semiclassical incoherent model, without increasing the computational complexity, by adding the single-atom quantum description of incoherent light emission for all the atoms. In a single stochastic realization of atomic positions, the incoherent scattering contribution to intensity from independent quantum-mechanical atoms $\propto \sum_j A_j(\langle\hat{\sigma}_{ee}^{(j)}\rangle - |\langle\hat{\sigma}_+^{(j)}\rangle|^2)$, where A_j encapsulates the light propagation effects (see "Methods" section)[66]. Augmenting the semiclassical model with this single-atom quantum description integrated over the sample yields the incoherent transmission $T_{\text{inc}}^{\text{SAQ}}$. The quantum effects of the incoherent signal solely due to many-body processes are then encapsulated in $T_{\text{inc}}^{\text{QM}} - T_{\text{inc}}^{\text{SAQ}}$.

The optical depth of the coherent transmission (Figs. 2a–c, 3a, c) corresponds physically to the degree to which extinction of the incident laser field by the averaged scattered field acts to reduce the transmission. The incoherent fluctuations in the scattered field (Figs. 2d–f, 3b) then counteract this reduction. In Fig. 2b, we identify many-body quantum fluctuations in the coherent transmission ($T_{\text{coh}}^{\text{QM}} - T_{\text{coh}}^{\text{SC}}$) that increase with increasing DD interaction (Fig. 3a, c), reaching normalized residuals of over 10% at $a = 0.25\lambda$ and $I \simeq I_{\text{sat}}$ (when the dipole amplitudes are greatest), where $I = 2\epsilon_0 c|\boldsymbol{\mathcal{E}}^+(\mathbf{r} = \mathbf{0})|^2$ is the peak incident laser intensity and $I_{\text{sat}} = 4\pi^2\hbar\gamma c/3\lambda^3$ is the saturation intensity. Remarkably, even for a fully random disk quantum effects on the scattering do not wash out, but can produce residuals between the models of a few percent. On the other hand, there are also regimes where $T_{\text{coh}}^{\text{SC}}$ accurately describes transmitted light. For example, in Fig. 3c the difference between $T_{\text{coh}}^{\text{QM}}$ and $T_{\text{coh}}^{\text{SC}}$ is less than 5% for $a \gtrsim 0.4\lambda$ or $I/I_{\text{sat}} \gtrsim 16$.
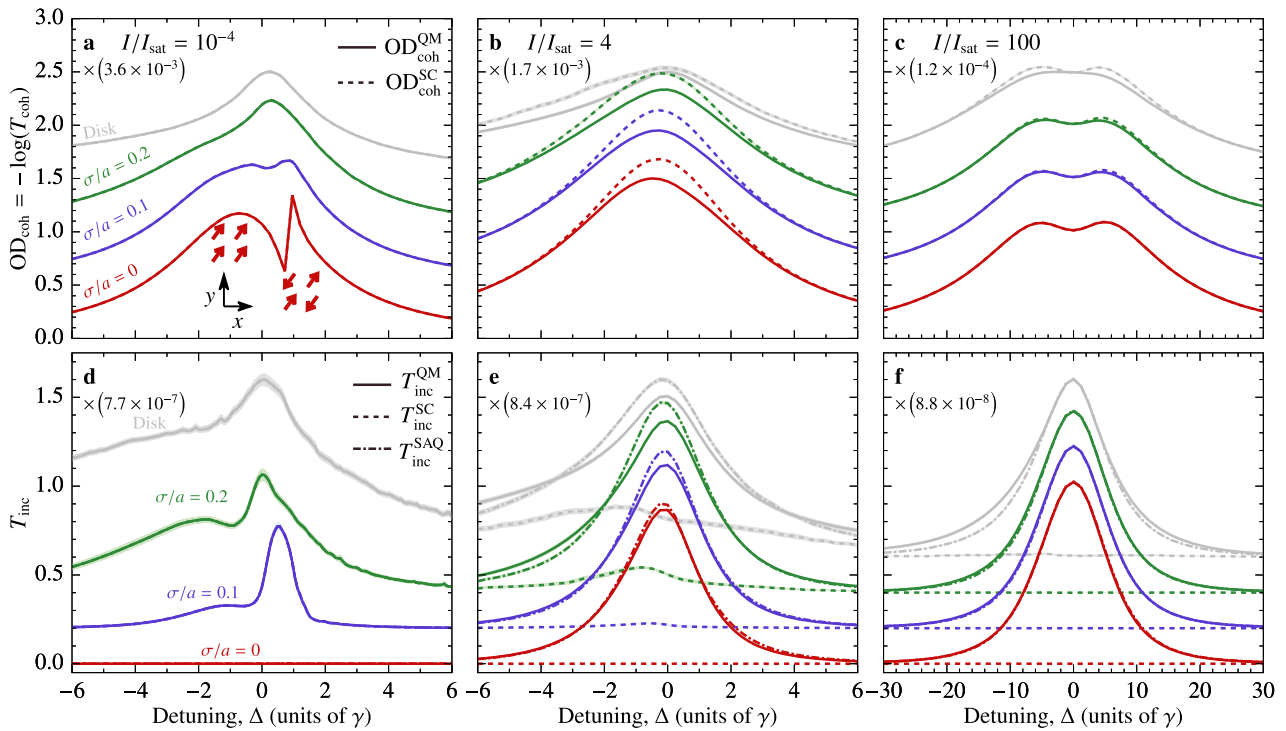
Fig. 2 Quantum effects in the optical transmission through a strongly coupled atomic ensemble. Curves for the coherent optical depth (**a–c**) and incoherent light transmission (**d–f**), from bottom to top: atoms in a 2 × 2 square array in the xy plane with lattice constant $a = 0.25\lambda$ and normally distributed position fluctuations (rms width $\sigma_{x,y}/a = 0$, 0.1, 0.2, respectively); and 4 atoms randomly distributed within a radius $R = 0.28\lambda$ (peak density $1.0k^3$) thin disk. The shaded regions show the standard sampling error of atomic position fluctuations. For clarity each line is offset from that below it by 0.5 (**a–c**) or 0.2 (**d–f**). Fluctuations in z are characterized by a $\sigma_z = 0.025\lambda$ normal distribution, except when atoms are fixed ($\sigma_{x,y} = \sigma_z = 0$). The incident beam has waist $w_0 = 10\lambda$, polarization $(\hat{\mathbf{x}} + \hat{\mathbf{y}})/\sqrt{2}$, and intensity $I/I_{sat} = 0.0001$ (**a**, **d**), $I/I_{sat} = 4$ (**b**, **e**), or $I/I_{sat} = 100$ (**c**, **f**). Red arrows in **a** show the atomic dipoles in the xy plane for the uniform superradiant and checkerboard-patterned subradiant eigenmodes.

In Fig. 3c we observe two distinct peaks in the quantum many-body signatures of the coherent scattering for $a = 0.25\lambda$. The peak at $\sqrt{I/I_{sat}} \approx 0.3$ results from a Fano interference between a narrow and an overlapping broad resonance (Fig. 3c inset), originating from an underlying highly subradiant (HWHM $= 0.1\gamma$) and superradiant (HWHM $= 2.7\gamma$) low light intensity eigenmode, respectively. The incident light couples to the phase-matched uniform superradiant eigenmode, but due to nonorthogonality of the non-Hermitian eigenmodes (Supplementary Note 3), the subradiant mode with rapid phase variation ("checkerboard" phase pattern, with dipoles at adjacent sites π out-of-phase) becomes populated at the narrow resonance (Fig. 2a). Strikingly, around this narrow resonance quantum effects constitute over 30% of the coherent scattering signal. We observe in Fig. 3c that, with increasing lattice spacing, the narrow Fano peak at $\sqrt{I/I_{sat}} \approx 0.3$ disappears, as the corresponding eigenmode becomes less subradiant.

In Fig. 2e, f, on the other hand, we see the incoherent transmission is almost entirely dominated by quantum fluctuations when $I \gtrsim I_{sat}$ ($T_{inc}^{SC} \to 0$). However, once we incorporate the single-atom quantum description into the scattering and therefore transmission T_{inc}^{SAQ}, the difference becomes much smaller and the many-body quantum fluctuations are, as with the coherent scattering, maximal around $I \sim I_{sat}$. Hence, using the improved model T_{inc}^{SAQ}, it is possible, even for incoherent scattering, to obtain excellent qualitative, and frequently quantitative agreement with the full quantum scattering (see Supplementary Note 4 for further demonstration of the different roles of quantum fluctuations in the incoherent scattering).

Spin correlations and entanglement. Up until now, we have identified many-body quantum effects via the transmitted light. These originate from the light-induced quantum correlations between internal levels of different atoms that do not satisfy the factorization assumption [given in Eq. (4)] of SCEs. In Fig. 4 we explicitly show these induced spin–spin correlations, and in Fig. 5a–c we show the many-body entanglement of formation (for a pair of atoms, using the formalism of ref. [67]—see Supplementary Note 5). The spin–spin correlations and entanglement exhibit behavior qualitatively similar to the quantum many-body correlations observed in the light scattering. As in Fig. 3c, both the correlations (Fig. 4) and entanglement (Fig. 5a–c) are maximal at $I \sim I_{sat}$, where the intensity at which this peak occurs and the peak's amplitude decrease for increasing atomic spacing. The correlations and entanglement also both manifest linesplitting for $I \gtrsim I_{sat}$, corresponding to when the atomic excited state population starts to increase. This is consistent with Fig. 2, where the observed quantum effects in transmitted light change from being maximal close to zero detuning when $I \sim I_{sat}$, to being maximal off resonance when $I \gg I_{sat}$. The purity of the atomic state (Fig. 5d) decreases to the limiting value 1/4 (Supplementary Note 5) for increasing I and is less sensitive to the array spacing than the entanglement E.

Large ensembles. When conditions are such that quantum effects on the light scattering are minimal, we can neglect quantum fluctuations, employing SCEs [Eqs. (5) and (6)] to analyze the coherent transmission through much larger ensembles, for which the full QME is inaccessible. In Fig. 6a–c we show how the
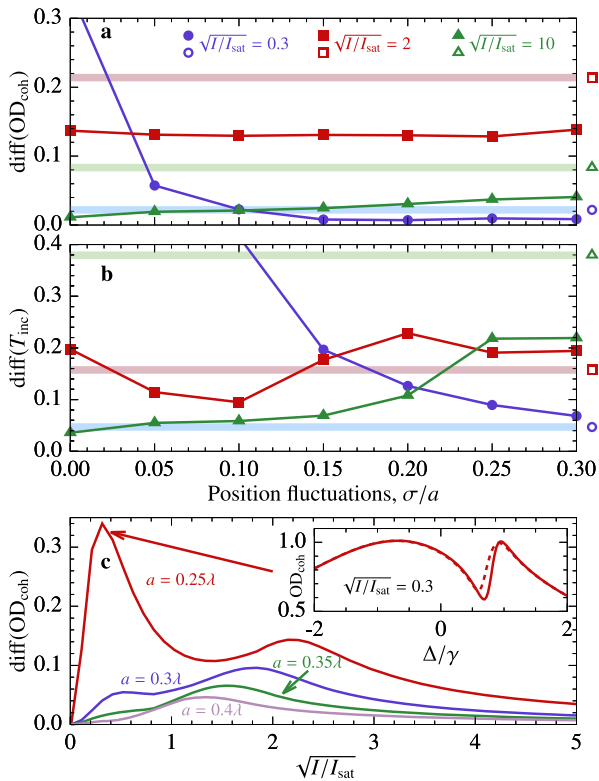
Fig. 4 Spin–spin correlations showing the emergence of light-induced quantum correlations and deviations from the semiclassical approximation. We calculate the one- and two-body spin expectations, $\rho_{ab}^{(j)}$ and $\rho_{ad;bc}^{(j,\ell)}$ respectively, for a 2 × 2 array with spacing $a = 0.25\lambda$ and atom indices (j, ℓ), as illustrated in **a**. For fixed atomic positions, the correlations are of solely quantum origin, occurring between internal levels of different atoms. **a** The correlation lineshape for increasing intensity $\sqrt{I/I_{sat}} = 1$ (red-dotted), 2 (blue-dashed), 5 (green-dot-dashed) exhibits an energy splitting. **b** The correlations peak around $I \sim I_{sat}$, tending to zero at very low and high light intensities. The behavior is qualitatively similar for other spin/atom pairs. The incident beam has waist $w_0 = 10\lambda$ and polarization $(\hat{\mathbf{x}} + \hat{\mathbf{y}})/\sqrt{2}$.

Fig. 3 Quantum many-body effects in optical transmission. a Relative differences, diff$(S) \equiv \max\{|S_{SCEs}(\Delta) - S_{QME}(\Delta)|/S_{QME}(\Delta)\}$, between quantum and semiclassical coherent optical depths (OD$_{coh}^{QM} = -\log(T_{coh}^{QM})$ and OD$_{coh}^{SC}$, respectively) for a 2 × 2 array with lattice constant $a = 0.25\lambda$ and normally distributed position fluctuations with varying rms width $\sigma_{x,y} = \sigma$, $\sigma_z = 0.025\lambda$ (solid markers and thin solid lines). The open markers and thick solid lines are for a disk of randomly distributed atoms with radius $R = 0.28\lambda$ and $\sigma_z = 0.025\lambda$. The light intensity is $\sqrt{I/I_{sat}} = 0.3$ (circles), 2 (squares), and 10 (triangles). **b** Relative differences between quantum and semiclassical (augmented by a single-atom quantum description) incoherent transmission, T_{inc}^{QM} and T_{inc}^{SAQ} respectively, for the same parameters as in **a**. **c** Relative differences between quantum and semiclassical coherent optical depth as a function of light intensity, for fixed atomic positions and for different spacings. The inset shows OD$_{coh}^{QM}$ (solid) and OD$_{coh}^{SC}$ (dashed) for a fixed array with $a = 0.25\lambda$ and $\sqrt{I/I_{sat}} = 0.3$. The incident beam has waist $w_0 = 10\lambda$, polarization $(\hat{\mathbf{x}} + \hat{\mathbf{y}})/\sqrt{2}$, and detuning $\Delta/\gamma \in [-4, 4]$ (**a**, **b**) and $\Delta/\gamma \in [-20, 20]$ (**c**).

Fig. 5 Entanglement of formation E and trace purity for a pair of atoms. a, **b** E (see ref. [67], Supplementary Note 5) for two atoms separated by $a = 0.25\lambda$ and polarized along the separation axis as a function of detuning and intensity [$\sqrt{I/I_{sat}} = 1$ (red-dotted), 1.5 (blue-dashed), and 2 (green-dot-dashed)]. The entanglement resonance splits for high intensities $I > I_{sat}$, and E is no longer maximal at the atomic resonance. **c** Similarly, the maximum entanglement decreases for increasing atomic spacing (decreasing interactions) [$a = 0.25\lambda$ (red-solid), 0.3λ (blue-dotted), and 0.35λ (green-dashed)], and peaks around $I = I_{sat}$, decreasing to 0 as $\sqrt{I/I_{sat}} \to 0$ or ∞. **d** The purity of the atomic state decreases to the limiting value $1/4$ (Supplementary Note 5) for increasing I and is less sensitive to the array spacing than E (spacings the same as in **c**). The black dot-dashed line shows the purity for a single atom.

transmission lineshapes of a 10 × 10 array differ significantly from the Lorentzian of independent atoms. For a single atom the linewidth is power broadened $\gamma_{PB}(I) = \gamma\sqrt{1 + I/I_{sat}}$. For spacings $a \gtrsim 0.3\lambda$, the coherent optical depth for a 10 × 10 interacting array can also be fitted well to a single Lorentzian (ignoring the small structure present at low light intensity due to interfering eigenmodes, Fig. 6a), with a linewidth which also scales with intensity. If the linewidth at low light intensity is superradiant (e.g., $a = 1.1\lambda$) or subradiant (e.g., $a = 0.8\lambda$), it will also be correspondingly larger or smaller than γ_{PB} for high intensities (Fig. 6c). For smaller spacings (e.g., $a = 0.25\lambda$), at high intensity the lineshape splits into a double resonance, producing a dip or "hole burning" (Fig. 6b). This dip is analogous to vacuum Rabi splitting[37,38], where the interatomic DD coupling has now taken the role of the cavity coupling. In cavity QED, the mirrors create images of an atom inside the cavity, mimicking a periodic array, and the resonance doublet can be understood as a splitting of the excited state (Supplementary Note 6). While the dip in Fig. 6b
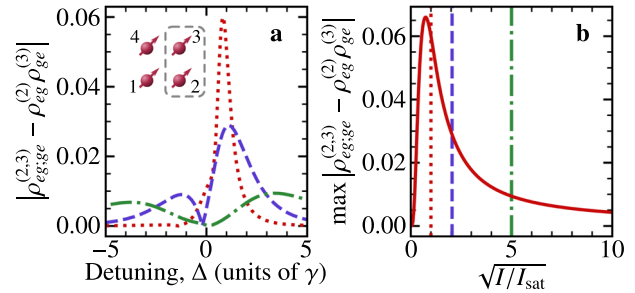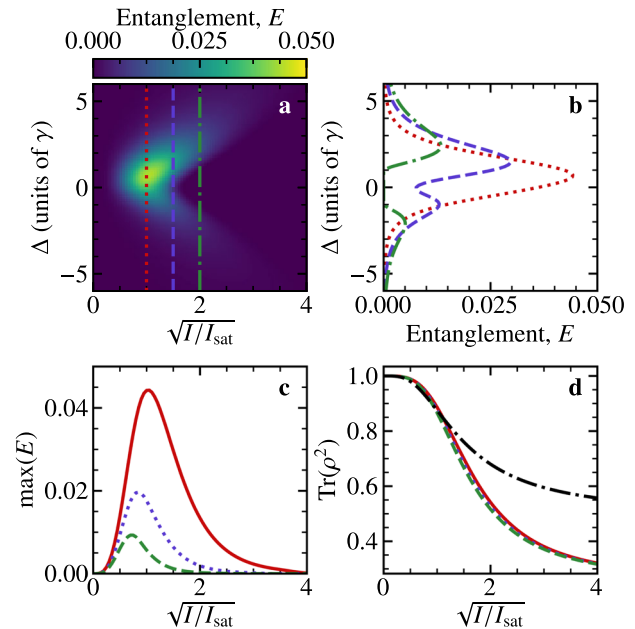
only occurs at sufficiently high density, it can interestingly still exist even in the fully random ensemble. With increasing light intensity, the incoherent scattering lineshape tends to that of the independent atom (Supplementary Note 7).
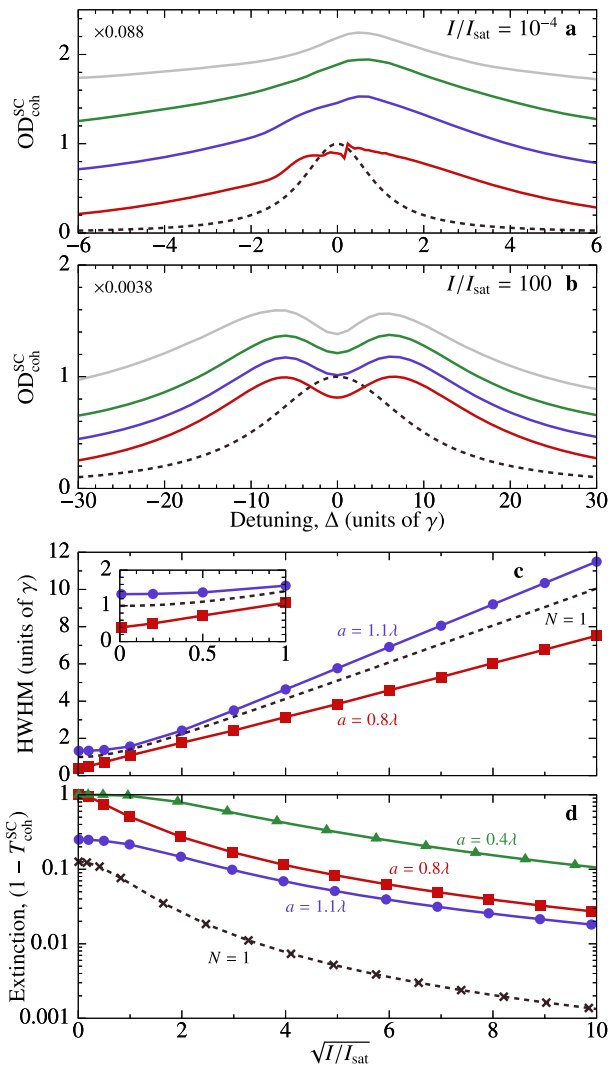
Fig. 6 Semiclassically evaluated optical depth, resonance Rabi splitting, power broadening, and maximum extinction for 100 atoms. a, b From bottom to top: semiclassical coherent optical depth OD_{coh}^{SC} for a 10×10 square array with lattice constant $a = 0.25\lambda$ and normally distributed position fluctuations (rms width $\sigma_{x,y}/a = 0, 0.1, 0.2$, respectively); and 100 atoms randomly distributed within a radius $R = 1.4\lambda$ (peak density $1.0k^3$) thin disk. The standard sampling errors (shaded regions) are too small to see. For clarity each line is offset from that below it by 0.5. Fluctuations in z are characterized by a $\sigma_z = 0.025\lambda$ normal distribution, except when atoms are fixed ($\sigma_{x,y} = \sigma_z = 0$). The incident beam has waist $w_0 = 10\lambda$, polarization $(\hat{\mathbf{x}} + \hat{\mathbf{y}})/\sqrt{2}$, and intensity $I/I_{sat} = 10^{-4}$ (**a**), and $I/I_{sat} = 100$ (**b**). Black dashed lines show normalized lineshapes for a single atom with power-broadened $\gamma_{PB} = \gamma(1 + I/I_{sat})^{1/2}$. **c** HWHM of OD_{coh}^{SC} for atoms at fixed positions with $a = 0.8\lambda$ (squares), 1.1λ (circles), and for a single atom (black dashed line). The beam ($w_0 = 30a$) is nearly uniform over the atoms and the light is collected over a solid angle $\sin\theta \lesssim 0.04$ ($a = 0.8\lambda$) and 0.03 ($a = 1.1\lambda$). **d** Peak extinction ($1 - T_{coh}^{SC}$) with fixed positions: $a = 0.8\lambda$ (squares), 1.1λ (circles), and 0.4λ (triangles). We set the beam waists to optimize extinction (3λ for $a/\lambda = 0.8, 1.1$ and 1.5λ for $a/\lambda = 0.4$) over a collection solid angle $\sin\theta \lesssim 0.37$ using circular polarization $-(\hat{\mathbf{x}} + i\hat{\mathbf{y}})/\sqrt{2}$.

A key feature of general subwavelength-spaced resonant emitter arrays is that they can exhibit perfect reflection[13,14], which may typically be modeled using point-dipole scatterers[15–17,19]. Dipolar planar arrays can act as cooperative antennae[68], with applications to quantum information processing[29], making understanding

nonlinear transmission essential. We calculate this for large arrays in Fig. 6d, and find that the reduction in the extinction as a function of light intensity is considerable—although less prominent with smaller spacings. This may ultimately restrict the application of atomic arrays as highly reflective cooperative mirrors to weak light intensities only.

Discussion

By comparing different descriptions of atom-light dynamics and light scattering, we have identified light-induced quantum effects, spin–spin correlations, and quantum entanglement in the light transmitted through planar arrays and disks which survive both position fluctuations and strong DD interactions. At narrow subradiant resonances, quantum fluctuations can be over 30%. Outside these resonances, provided we improve the model by incorporating the single-atom quantum description, SCEs typically still reproduce, also for incoherent scattering, the full quantum behavior at least qualitatively. This provides a methodology to calculate transmission of light through large arrays, consisting of hundreds of atoms, which can exhibit striking many-body phenomena (even without any quantum effects) reminiscent of single-atom power broadening and vacuum Rabi splitting. The existence of many-body quantum effects despite strong driving, high densities, and even with significant atomic position fluctuations is surprising. It suggests that optical quantum information processing in atomic ensembles[4] need not necessarily be restricted to dilute systems. Subradiant resonance narrowing has now been experimentally observed in the transmitted light through an optical lattice of atoms in a Mott-insulator state in the classical limit of low light intensity[69]. Several of our findings could also be verified in this setup by increasing the intensity of the incident light. The presence, even in uniform disks, of many-body effects attracting considerable interest[1,2,49,70] further relaxes the conditions necessary for their experimental observation.

Methods

Dynamics and correlation functions. We simulate the optical response of N-atom ensembles by stochastically sampling fixed positions $\{\mathbf{r}_1, ..., \mathbf{r}_N\}$ of stationary atoms, as the atomic center-of-mass dynamics are assumed negligible. In the full quantum dynamics, for each stochastic realization we solve the equations of motion for the N-atom density matrix $\rho_{\{\mathbf{r}_1,...,\mathbf{r}_N\}}(t)$ with the atoms at fixed positions $\{\mathbf{r}_1, ..., \mathbf{r}_N\}$, obeying QME [Eq. (2)]. In the Hamiltonian in Eq. (3) we use slowly-varying field amplitudes and atomic variables where the rapid rotation at the laser frequency ω has been factored out by substitutions $\mathcal{E}^+ e^{i\omega t} \rightarrow \mathcal{E}^+$, $\hat{\sigma}^{(j)}(t) e^{i\omega t} \rightarrow \hat{\sigma}^{(j)}(t)$, etc. The collective coupling matrices $\Omega_{j\ell}$ and $\gamma_{j\ell}$, resulting, respectively, in collective resonance line shifts and linewidths in Eq. (2) (see Supplementary Note 3), are the real and imaginary parts of the dipole radiation kernel $\mathsf{G}(\mathbf{r})$:

$$\frac{1}{\hbar\epsilon_0}\mathbf{d}_{eg} \cdot \left[\mathsf{G}(\mathbf{r}_j - \mathbf{r}_\ell)\mathbf{d}_{ge}\right] = \Omega_{j\ell} + i\gamma_{j\ell}, \quad (7)$$

where

$$\mathsf{G}(\mathbf{r})\hat{\mathbf{d}} = \frac{k^3}{4\pi}\left\{(\hat{\mathbf{n}} \times \hat{\mathbf{d}}) \times \hat{\mathbf{n}}\frac{e^{ikr}}{kr} + [3\hat{\mathbf{n}}(\hat{\mathbf{n}} \cdot \hat{\mathbf{d}}) - \hat{\mathbf{d}}]\left[\frac{1}{(kr)^3} - \frac{i}{(kr)^2}\right]e^{ikr}\right\} - \frac{\hat{\mathbf{d}}\,\delta(\mathbf{r})}{3} \quad (8)$$

is the electric field amplitude for an oscillating electric dipole $\hat{\mathbf{d}}$ at the origin and $\hat{\mathbf{n}} = \mathbf{r}/r$. Note that we typically drop the contact interaction term[36].

Once $\rho_{\{\mathbf{r}_1,...,\mathbf{r}_N\}}(t)$ is known, the one-body $\rho_{ab}^{(j)}$ (jth atom), two-body $\rho_{ad;bc}^{(j,\ell)}$ (jth and ℓth atoms), etc., expectation values for this stochastic realization are given by:

$$\rho_{ge}^{(j)} = \left\langle\hat{\sigma}_-^{(j)}\right\rangle = \mathrm{Tr}\left\{\hat{\sigma}_-^{(j)}\rho_{\{\mathbf{r}_1,...,\mathbf{r}_N\}}\right\}, \quad (9)$$

$$\rho_{ee}^{(j)} = 1 - \rho_{gg}^{(j)} = \left\langle\hat{\sigma}_{ee}^{(j)}\right\rangle = \mathrm{Tr}\left\{\hat{\sigma}_{ee}^{(j)}\rho_{\{\mathbf{r}_1,...,\mathbf{r}_N\}}\right\}, \quad (10)$$

$$\rho_{ge;eg}^{(j,\ell)} = \left\langle\hat{\sigma}_-^{(j)}\hat{\sigma}_+^{(\ell)}\right\rangle(1 - \delta_{j\ell}) = \mathrm{Tr}\left\{\hat{\sigma}_-^{(j)}\hat{\sigma}_+^{(\ell)}\rho_{\{\mathbf{r}_1,...,\mathbf{r}_N\}}\right\}(1 - \delta_{j\ell}), \quad (11)$$

and so forth. Here $\rho_{ge}^{(j)}$ represents the correlations $\langle\hat{\psi}_g^\dagger\hat{\psi}_e\rangle$ of Eq. (14), and corresponds to the matrix element $\langle e|\rho_1|g\rangle$ of the one-body density matrix ρ_1.

In each stochastic realization, the N-atom configuration of positions $\{\mathbf{r}_1, \ldots, \mathbf{r}_N\}$ is obtained by sampling from a joint probability distribution $P(\mathbf{r}_1, \ldots, \mathbf{r}_N)$, taken to be the initial distribution of stationary atoms. Ensemble-averaging over many such realizations then transforms the expectation values $\rho_{ab}^{(j)}(t)$, $\rho_{ad;bc}^{(j,\ell)}(t)$, etc., to spatial correlation functions for the atoms at any given time t:

$$\left\langle \hat{\psi}_a^\dagger(\mathbf{r}, t)\hat{\psi}_b(\mathbf{r}, t) \right\rangle = \int d^3r_1 \ldots d^3r_N \left\langle \hat{\psi}_a^\dagger(\mathbf{r}, t)\hat{\psi}_b(\mathbf{r}, t) \right\rangle_{\{\mathbf{r}_1, \ldots, \mathbf{r}_N\}} P(\mathbf{r}_1, \ldots, \mathbf{r}_N),$$

$$(12)$$

$$\left\langle \hat{\psi}_a^\dagger(\mathbf{r}, t)\hat{\psi}_b^\dagger(\mathbf{r}', t)\hat{\psi}_c(\mathbf{r}', t)\hat{\psi}_d(\mathbf{r}, t) \right\rangle$$
$$= \int d^3r_1 \ldots d^3r_N \left\langle \hat{\psi}_a^\dagger(\mathbf{r}, t)\hat{\psi}_b^\dagger(\mathbf{r}', t)\hat{\psi}_c(\mathbf{r}', t)\hat{\psi}_d(\mathbf{r}, t) \right\rangle_{\{\mathbf{r}_1, \ldots, \mathbf{r}_N\}} P(\mathbf{r}_1, \ldots, \mathbf{r}_N),$$

$$(13)$$

and so-forth for higher-order correlations. The atomic correlation functions for a single realization of fixed atomic positions are given in terms of $\rho_{ab}^{(j)}$ and $\rho_{ad;bc}^{(j,\ell)}$ by

$$\left\langle \hat{\psi}_a^\dagger(\mathbf{r}, t)\hat{\psi}_b(\mathbf{r}, t) \right\rangle_{\{\mathbf{r}_1, \ldots, \mathbf{r}_N\}} = \sum_j \rho_{ab}^{(j)}(t)\delta(\mathbf{r} - \mathbf{r}_j),$$

$$(14)$$

$$\left\langle \hat{\psi}_a^\dagger(\mathbf{r}, t)\hat{\psi}_b^\dagger(\mathbf{r}', t)\hat{\psi}_c(\mathbf{r}', t)\hat{\psi}_d(\mathbf{r}, t) \right\rangle_{\{\mathbf{r}_1, \ldots, \mathbf{r}_N\}} = \sum_{j\ell} \rho_{ad;bc}^{(j,\ell)}(t)\delta(\mathbf{r} - \mathbf{r}_j)\delta(\mathbf{r}' - \mathbf{r}_\ell),$$

$$(15)$$

and it is through solving the coupled dynamics between the light and atoms for each stochastic run and ensemble-averaging over many such realizations that we establish the light-induced spatial correlations between atoms[36,55].

For a single, isolated atom at the laser focus, the solutions to Eqs. (5), (6) (i.e., the optical Bloch equations) in the steady state are

$$\rho_{ge} = \frac{\mathbf{d}_{eg} \cdot \boldsymbol{\mathcal{E}}^+(0)}{\hbar} \frac{-\Delta + i\gamma}{\Delta^2 + \gamma^2(1 + I/I_{sat})},$$

$$(16)$$

$$\rho_{ee} = \frac{I}{I_{sat}} \frac{\gamma^2/2}{\Delta^2 + \gamma^2(1 + I/I_{sat})},$$

$$(17)$$

where $I/I_{sat} = 2|\mathbf{d}_{eg} \cdot \boldsymbol{\mathcal{E}}^+(0)|^2/(\hbar\gamma)^2$. The effective linewidth in the denominators of Eqs. (16) and (17) is now power broadened, i.e., $\gamma_{PB} = \gamma\sqrt{1 + I/I_{sat}}$.

We compare the full quantum solution of QME [Eq. (2)] with SCEs [Eqs. (5) and (6)] for the one-body terms $\rho_{ab}^{(j)}$ based on the factorization $\rho_{ad;bc}^{(j)} \simeq \rho_{ad}^{(j)}\rho_{bc}^{(\ell)}$, which neglects quantum fluctuations. In terms of the stochastic sampling procedure, we express this semiclassical factorization as:

$$\left\langle \hat{\psi}_a^\dagger(\mathbf{r})\hat{\psi}_b^\dagger(\mathbf{r}')\hat{\psi}_c(\mathbf{r}')\hat{\psi}_d(\mathbf{r}) \right\rangle_{SC} = \int d^3r_1 \ldots d^3r_N$$
$$\left\langle \hat{\psi}_a^\dagger(\mathbf{r})\hat{\psi}_d(\mathbf{r}) \right\rangle_{\{\mathbf{r}_1, \ldots, \mathbf{r}_N\}} \left\langle \hat{\psi}_b^\dagger(\mathbf{r}')\hat{\psi}_c(\mathbf{r}') \right\rangle_{\{\mathbf{r}_1, \ldots, \mathbf{r}_N\}} P(\mathbf{r}_1, \ldots, \mathbf{r}_N)[1 - \delta(\mathbf{r} - \mathbf{r}')],$$

$$(18)$$

where the $[1 - \delta(\mathbf{r} - \mathbf{r}')]$ term is necessary to exclude the case where the annihilation operators refer twice to the same atom. Despite the factorization of the internal atomic correlation functions, we generally have $\langle \hat{\psi}_a^\dagger(\mathbf{r})\hat{\psi}_b^\dagger(\mathbf{r}')\hat{\psi}_c(\mathbf{r}')\hat{\psi}_d(\mathbf{r}) \rangle_{SC} \neq \langle \hat{\psi}_a^\dagger(\mathbf{r})\hat{\psi}_d(\mathbf{r}) \rangle\langle \hat{\psi}_b^\dagger(\mathbf{r}')\hat{\psi}_c(\mathbf{r}') \rangle$, as the fluctuations of the atomic positions that are included in SCEs approach can result in strong light-induced correlations.

In general for the atomic distribution before the light enters the sample we have $P(\mathbf{r}_1, \ldots, \mathbf{r}_N) = |\Psi(\mathbf{r}_1, \ldots, \mathbf{r}_N)|^2$, where $\Psi(\mathbf{r}_1, \ldots, \mathbf{r}_N)$ denotes the N-body atomic wave function in position representation. For the initially uncorrelated atoms, each atom is sampled independently. We consider two different geometries: (i) atoms trapped in a two-dimensional array with precisely one atom per site; and (ii) a random, uniform distribution of atoms inside a thin, cylindrical disk of radius R and thickness Z. For the former case, we can sample the stochastic position of an atom in each site[10], obtaining $P(\mathbf{r}_1, \ldots, \mathbf{r}_N) = \varrho_1(\mathbf{r}_1)\ldots\varrho_N(\mathbf{r}_N)$, where the density distribution of the jth array site, centered at $\mathbf{r}_j = \mathbf{R}_j$, is approximated by a Gaussian:

$$\varrho_j(\mathbf{r}_j) = \frac{1}{\sqrt{8\pi^3}\sigma_x\sigma_y\sigma_z}\exp\left(-\frac{[x_j - X_j]^2}{2\sigma_x^2} - \frac{[y_j - Y_j]^2}{2\sigma_y^2} - \frac{[z_j - Z_j]^2}{2\sigma_z^2}\right),$$

$$(19)$$

where the standard deviations $\sigma_x, \sigma_y, \sigma_z$ quantify the spatial confinement of the trapped atoms in all three directions.

Scattered light. The total electric field operator $\hat{\mathbf{E}}^\pm(\mathbf{r}) = \boldsymbol{\mathcal{E}}^\pm(\mathbf{r}) + \hat{\mathbf{E}}_d^\pm(\mathbf{r})$ is the sum of the laser field and the fields scattered from all atoms

$$\epsilon_0\hat{\mathbf{E}}_d^+(\mathbf{r}) = \int d^3\mathcal{R}\, \mathsf{G}(\mathbf{r} - \boldsymbol{\mathcal{R}})\hat{\mathbf{P}}^+(\boldsymbol{\mathcal{R}}).$$

$$(20)$$

To analyze the different contributions in the scattered light, we write it as $\hat{\mathbf{E}}_d^+ = \langle \hat{\mathbf{E}}_d^+ \rangle + \delta\hat{\mathbf{E}}_d^+$, where $\delta\hat{\mathbf{E}}_d^+$ denotes the fluctuations. We then obtain,

$$\langle \hat{\mathbf{E}}^-(\mathbf{r})\hat{\mathbf{E}}^+(\mathbf{r}) \rangle = \boldsymbol{\mathcal{E}}^-(\mathbf{r})\boldsymbol{\mathcal{E}}^+(\mathbf{r}) + \boldsymbol{\mathcal{E}}^-(\mathbf{r})\langle \hat{\mathbf{E}}_d^+(\mathbf{r}) \rangle + \langle \hat{\mathbf{E}}_d^-(\mathbf{r}) \rangle\boldsymbol{\mathcal{E}}^+(\mathbf{r}) + \langle \hat{\mathbf{E}}_d^-(\mathbf{r}) \rangle\langle \hat{\mathbf{E}}_d^+(\mathbf{r}) \rangle$$
$$+ \langle \delta\hat{\mathbf{E}}_d^-(\mathbf{r})\delta\hat{\mathbf{E}}_d^+(\mathbf{r}) \rangle;$$

$$(21)$$

here $\hat{\mathbf{E}}^-\hat{\mathbf{E}}^+$ is a dyadic product with elements $\hat{E}_\alpha^-\hat{E}_\beta^+$, with $\alpha, \beta \in \{1, 2, 3\}$ cycling over the different polarization components, where the intensity is proportional to its diagonal elements. The first term on the right hand side of Eq. (21) yields the incident light intensity, the second, third, and fourth terms produce the coherent scattering, and the final term produces incoherent scattering dependent on fluctuations. Rearranging Eq. (21) to solve for the incoherent scattering gives:

$$\langle \delta\hat{\mathbf{E}}_d^-(\mathbf{r})\, \delta\hat{\mathbf{E}}_d^+(\mathbf{r}) \rangle = \langle \hat{\mathbf{E}}_d^-(\mathbf{r})\, \hat{\mathbf{E}}_d^+(\mathbf{r}) \rangle - \langle \hat{\mathbf{E}}_d^-(\mathbf{r}) \rangle\langle \hat{\mathbf{E}}_d^+(\mathbf{r}) \rangle,$$

$$(22)$$

which describes correlations in the scattered light.

Consider first a single atom at the origin $\boldsymbol{\mathcal{R}} = 0$. According to Eq. (20), the coherently scattered light consists of expectation values

$$\left\langle \hat{\mathbf{E}}_d^+(\mathbf{r}) \right\rangle = \frac{1}{\epsilon_0}\left[\mathsf{G}(\mathbf{r})\mathbf{d}_{ge}\right]\langle \hat{\sigma}_- \rangle,$$

$$(23)$$

and there is no difference between the quantum and semiclassical coherent scattering. Hence, any difference between the quantum and semiclassical coherent scattering for a many-atom ensemble is due solely to many-body quantum effects. The incoherent contribution in Eq. (22) is more subtle, as

$$\left\langle \hat{\mathbf{E}}_d^-(\mathbf{r})\hat{\mathbf{E}}_d^+(\mathbf{r}) \right\rangle = \frac{1}{\epsilon_0^2}\left[\mathsf{G}(\mathbf{r})\mathbf{d}_{ge}\right]^*\left[\mathsf{G}(\mathbf{r})\mathbf{d}_{ge}\right]\langle \hat{\sigma}_+\hat{\sigma}_- \rangle$$

$$(24)$$

means the incoherently scattered light from a single atom yields

$$\left\langle \delta\hat{\mathbf{E}}_d^-(\mathbf{r})\delta\hat{\mathbf{E}}_d^+(\mathbf{r}) \right\rangle = \frac{1}{\epsilon_0^2}\left[\mathsf{G}(\mathbf{r})\mathbf{d}_{ge}\right]^*\left[\mathsf{G}(\mathbf{r})\mathbf{d}_{ge}\right]\left(\langle \hat{\sigma}_{ee} \rangle - |\langle \hat{\sigma}_+ \rangle|^2\right),$$

$$(25)$$

where we have used $\hat{\sigma}_+\hat{\sigma}_- = \hat{\sigma}_{ee}$. In the semiclassical approximation, where the quantum fluctuations are ignored, one then replaces $\hat{\sigma}_+$ by $\langle \hat{\sigma}_+ \rangle$ in Eq. (24)[66], such that

$$\left\langle \hat{\mathbf{E}}_d^-(\mathbf{r})\hat{\mathbf{E}}_d^+(\mathbf{r}) \right\rangle_{SC} = \frac{1}{\epsilon_0^2}\left[\mathsf{G}(\mathbf{r})\mathbf{d}_{ge}\right]^*\left[\mathsf{G}(\mathbf{r})\mathbf{d}_{ge}\right]|\langle \hat{\sigma}_+ \rangle|^2,$$

$$(26)$$

and the incoherently scattered light intensity in Eq. (25) vanishes. Unlike the coherent scattering, the incoherent scattering for a single atom therefore differs depending on whether we treat it in a quantum or semiclassical manner.

Generalizing to the many-atom case, Eq. (24) now becomes

$$\left\langle \hat{\mathbf{E}}_d^-(\mathbf{r})\hat{\mathbf{E}}_d^+(\mathbf{r}) \right\rangle = \frac{1}{\epsilon_0^2}\int d^3\boldsymbol{\mathcal{R}}d^3\boldsymbol{\mathcal{R}}'[\mathsf{G}(\mathbf{r} - \boldsymbol{\mathcal{R}})]^*[\mathsf{G}(\mathbf{r} - \boldsymbol{\mathcal{R}}')]\left\langle \hat{\mathbf{P}}^-(\boldsymbol{\mathcal{R}})\hat{\mathbf{P}}^+(\boldsymbol{\mathcal{R}}') \right\rangle,$$

$$(27)$$

where, as in Eq. (20), $[\mathsf{G}(\mathbf{r} - \boldsymbol{\mathcal{R}})]^*$ acts on $\hat{\mathbf{P}}^-(\boldsymbol{\mathcal{R}})$ and likewise $\mathsf{G}(\mathbf{r} - \boldsymbol{\mathcal{R}}')$ on $\hat{\mathbf{P}}^+(\boldsymbol{\mathcal{R}}')$. When calculating the full quantum solution, the correlation functions are evaluated using the solution to QME [Eq. (2)] and by ensemble-averaging over many realizations of atomic positions. However, we can also introduce the many-body version of the single-atom semiclassical approximation [Eq. (26)] to light scattering:

$$\left\langle \hat{\mathbf{P}}^-(\boldsymbol{\mathcal{R}})\hat{\mathbf{P}}^+(\boldsymbol{\mathcal{R}}') \right\rangle \simeq \int d^3r_1 \ldots d^3r_N \left\langle \hat{\mathbf{P}}^-(\boldsymbol{\mathcal{R}}) \right\rangle_{\{\mathbf{r}_1, \ldots, \mathbf{r}_N\}}$$
$$\left\langle \hat{\mathbf{P}}^+(\boldsymbol{\mathcal{R}}') \right\rangle_{\{\mathbf{r}_1, \ldots, \mathbf{r}_N\}} P(\mathbf{r}_1, \ldots, \mathbf{r}_N),$$

$$(28)$$

substituting this back into Eq. (27) to give the semiclassical scattered field

$$\left\langle \hat{\mathbf{E}}_d^-(\mathbf{r})\hat{\mathbf{E}}_d^+(\mathbf{r}) \right\rangle_{SC} = \frac{1}{\epsilon_0^2}\int d^3\boldsymbol{\mathcal{R}}d^3\boldsymbol{\mathcal{R}}'[\mathsf{G}(\mathbf{r} - \boldsymbol{\mathcal{R}})]^*[\mathsf{G}(\mathbf{r} - \boldsymbol{\mathcal{R}}')]$$
$$\int d^3r_1 \ldots d^3r_N \left\langle \hat{\mathbf{P}}^-(\boldsymbol{\mathcal{R}}) \right\rangle_{\{\mathbf{r}_1, \ldots, \mathbf{r}_N\}}$$
$$\left\langle \hat{\mathbf{P}}^+(\boldsymbol{\mathcal{R}}') \right\rangle_{\{\mathbf{r}_1, \ldots, \mathbf{r}_N\}} P(\mathbf{r}_1, \ldots, \mathbf{r}_N).$$

$$(29)$$

Deriving the semiclassical scattered light in Eq. (29) corresponds to a systematic way of neglecting all quantum fluctuations when the atomic response is first calculated from SCEs [Eqs. (5) and (6)]. Hence, comparing the scattered light of Eq. (29) with the equivalent full quantum solution of Eq. (27) provides a signature for quantum effects in the collective atomic response. Alternatively, if our goal is to determine a computationally efficient and accurate approximation to the full quantum solution, we can instead try to improve the semiclassical approximation. A simple way to achieve this without increasing computational demands is to include the single-atom quantum description to incoherent scattering [Eq. (25)] integrated over the extent of the sample, which is sufficient in a number of cases to capture the leading quantum contributions.

We begin this procedure by placing the atomic operators in Eq. (27) in the normal order. This yields for the expectation term on the right hand side of

Eq. (27) (for both fermionic and bosonic atoms)

$$\left\langle \hat{\psi}_e^\dagger(\boldsymbol{\mathcal{R}})\hat{\psi}_g(\boldsymbol{\mathcal{R}})\hat{\psi}_g^\dagger(\boldsymbol{\mathcal{R}}')\hat{\psi}_e(\boldsymbol{\mathcal{R}}')\right\rangle = \left\langle \hat{\psi}_e^\dagger(\boldsymbol{\mathcal{R}})\hat{\psi}_e(\boldsymbol{\mathcal{R}}')\right\rangle\delta(\boldsymbol{\mathcal{R}}-\boldsymbol{\mathcal{R}}')$$
$$+ \left\langle \hat{\psi}_e^\dagger(\boldsymbol{\mathcal{R}})\hat{\psi}_g^\dagger(\boldsymbol{\mathcal{R}}')\hat{\psi}_e(\boldsymbol{\mathcal{R}}')\hat{\psi}_g(\boldsymbol{\mathcal{R}})\right\rangle. \quad (30)$$

Substituting this into Eq. (27) and using the semiclassical factorization approximation of Eq. (18) we obtain

$$\left\langle \hat{\mathbf{E}}_d^-(\mathbf{r})\hat{\mathbf{E}}_d^+(\mathbf{r})\right\rangle_{SAQ} = \frac{1}{\epsilon_0^2}\int d^3\boldsymbol{\mathcal{R}}\left[\mathbf{G}(\mathbf{r}-\boldsymbol{\mathcal{R}})\mathbf{d}_{ge}\right]^*\left[\mathbf{G}(\mathbf{r}-\boldsymbol{\mathcal{R}})\mathbf{d}_{ge}\right]\left\langle \hat{\psi}_e^\dagger(\boldsymbol{\mathcal{R}})\hat{\psi}_e(\boldsymbol{\mathcal{R}})\right\rangle$$
$$+ \frac{1}{\epsilon_0^2}\int' d^3\boldsymbol{\mathcal{R}}d^3\boldsymbol{\mathcal{R}}'\left\{[\mathbf{G}(\mathbf{r}-\boldsymbol{\mathcal{R}})]^*[\mathbf{G}(\mathbf{r}-\boldsymbol{\mathcal{R}}')]\right.$$
$$\int d^3r_1\ldots d^3r_N\left\langle \hat{\mathbf{P}}^-(\boldsymbol{\mathcal{R}})\right\rangle_{\{\mathbf{r}_1,\ldots,\mathbf{r}_N\}}$$
$$\left.\left\langle \hat{\mathbf{P}}^+(\boldsymbol{\mathcal{R}}')\right\rangle_{\{\mathbf{r}_1,\ldots,\mathbf{r}_N\}}P(\mathbf{r}_1,\ldots,\mathbf{r}_N)\right\}, \quad (31)$$

where $\int'$ denotes a double integral over all $\{\boldsymbol{\mathcal{R}},\boldsymbol{\mathcal{R}}'\}$ excluding $\boldsymbol{\mathcal{R}}=\boldsymbol{\mathcal{R}}'$. The difference between this augmented (semiclassical plus single-atom quantum) expression and the semiclassical expression of Eq. (29) in the scattered intensity is effectively the contributions of the single atom incoherent (quantum) scattering from Eq. (25) integrated over the extent of the sample:

$$\left\langle \hat{\mathbf{E}}_d^-(\mathbf{r})\hat{\mathbf{E}}_d^+(\mathbf{r})\right\rangle_{SAQ} - \left\langle \hat{\mathbf{E}}_d^-(\mathbf{r})\hat{\mathbf{E}}_d^+(\mathbf{r})\right\rangle_{SC}$$
$$= \frac{1}{\epsilon_0^2}\int d^3\boldsymbol{\mathcal{R}}\left[\mathbf{G}(\mathbf{r}-\boldsymbol{\mathcal{R}})\mathbf{d}_{ge}\right]^*\left[\mathbf{G}(\mathbf{r}-\boldsymbol{\mathcal{R}})\mathbf{d}_{ge}\right]\left\langle \hat{\psi}_e^\dagger(\boldsymbol{\mathcal{R}})\hat{\psi}_e(\boldsymbol{\mathcal{R}})\right\rangle$$
$$- \frac{1}{\epsilon_0^2}\int d^3\boldsymbol{\mathcal{R}}\left\{[\mathbf{G}(\mathbf{r}-\boldsymbol{\mathcal{R}})]^*[\mathbf{G}(\mathbf{r}-\boldsymbol{\mathcal{R}})]\right.$$
$$\left.\int d^3r_1\ldots d^3r_N\left\langle \hat{\mathbf{P}}^-(\boldsymbol{\mathcal{R}})\right\rangle_{\{\mathbf{r}_1,\ldots,\mathbf{r}_N\}}\left\langle \hat{\mathbf{P}}^+(\boldsymbol{\mathcal{R}})\right\rangle_{\{\mathbf{r}_1,\ldots,\mathbf{r}_N\}}P(\mathbf{r}_1,\ldots,\mathbf{r}_N)\right\}. \quad (32)$$

This improved description includes both the semiclassical contribution and the single-body quantum fluctuations, meaning any difference in the incoherent scattering between this improved model and the full quantum model is solely due to many-body quantum effects.

Transmission. Coherently and incoherently transmitted light is calculated through a disk of cross-sectional area S perpendicular to the optical axis a distance $f = 500\lambda$ downstream of the atoms. We consider light transmitted in the same spatial mode as the driving field, motivated by a typical experimental scheme of collecting transmitted light into a single-mode optical fiber, although, for simplicity, we ignore any explicit refocussing or fiber coupling. The transmitted light therefore has the form

$$T = \frac{\int dS \int dS' \boldsymbol{\mathcal{E}}^+(\mathbf{r})\cdot\left\langle \hat{\mathbf{E}}^-(\mathbf{r})\hat{\mathbf{E}}^+(\mathbf{r}')\right\rangle\cdot\boldsymbol{\mathcal{E}}^-(\mathbf{r}')}{\left|\int dS\,\boldsymbol{\mathcal{E}}^+(\mathbf{r})\cdot\boldsymbol{\mathcal{E}}^-(\mathbf{r})\right|^2}. \quad (33)$$

Note that because of the double integral over S and S' the expectation term is now a function of $\mathbf{r}$ and $\mathbf{r}'$, although substituting $\mathbf{r}'$ into the preceding equations does not affect our discussion of coherent and incoherent scattering.

To calculate the coherent transmission T_{coh} (plotted as optical depth $OD_{coh} \equiv -\log T_{coh}$), we substitute the first four terms on the right hand side of Eqs. (21) into (33). This gives quantum T_{coh}^{QM} or semiclassical T_{coh}^{SC} coherent transmission, depending on whether we use the solutions to QME or SCEs . To calculate the incoherent contribution to the transmission, we replace the two-field expectation in Eqs. (33) with (22). Evaluating Eq. (22) using Eqs. (27) and (30), along with the solutions to QME , results in the quantum incoherent transmission T_{inc}^{QM}. Using instead the solutions to SCEs and either Eqs. (29) or (31), respectively, produces the semiclassical incoherent transmission T_{inc}^{SC}, or the improved model for incoherent transmission T_{inc}^{SAQ} where the independent-atom quantum description is added to the semiclassical model.

Data availability

References
1. Javanainen, J., Ruostekoski, J., Li, Y. & Yoo, S.-M. Shifts of a resonance line in a dense atomic sample. *Phys. Rev. Lett.* **112**, 113603 (2014).
2. Javanainen, J. & Ruostekoski, J. Light propagation beyond the mean-field theory of standard optics. *Opt. Express* **24**, 993 (2016).
3. Mollow, B. R. Power spectrum of light scattered by two-level systems. *Phys. Rev.* **188**, 1969–1975 (1969).
4. Hammerer, K., Sørensen, A. S. & Polzik, E. S. Quantum interface between light and atomic ensembles. *Rev. Mod. Phys.* **82**, 1041–1093 (2010).
5. Friedberg, R., Hartmann, S. & Manassah, J. Frequency shifts in emission and absorption by resonant systems ot two-level atoms. *Phys. Rep.* **7**, 101–179 (1973).
6. Scully, M. O. & Svidzinsky, A. A. The lamb shift—yesterday, today, and tomorrow. *Science* **328**, 1239–1241 (2010).
7. Röhlsberger, R., Schlage, K., Sahoo, B., Couet, S. & Rüffer, R. Collective Lamb shift in single-photon superradiance. *Science* **328**, 1248–1251 (2010).
8. Guerin, W., Rouabah, M. & Kaiser, R. Light interacting with atomic ensembles: collective, cooperative and mesoscopic effects. *J. Mod. Opt.* **64**, 895–907 (2017).
9. Lemoult, F., Lerosey, G., de Rosny, J. & Fink, M. Resonant metalenses for breaking the diffraction barrier. *Phys. Rev. Lett.* **104**, 203901 (2010).
10. Jenkins, S. D. & Ruostekoski, J. Controlled manipulation of light by cooperative response of atoms in an optical lattice. *Phys. Rev. A* **86**, 031602 (2012).
11. Perczel, J. et al. Photonic band structure of two-dimensional atomic lattices. *Phys. Rev. A* **96**, 063801 (2017).
12. Bettles, R. J., Minár, J., Adams, C. S., Lesanovsky, I. & Olmos, B. Topological properties of a dense atomic lattice gas. *Phys. Rev. A* **96**, 041603 (2017).
13. Tretyakov, S. *Analytical Modeling in Applied Electromagnetics*. (Artech House, Norwood, MA, 2003).
14. García de Abajo, F. J. Colloquium: light scattering by particle and hole arrays. *Rev. Mod. Phys.* **79**, 1267–1290 (2007).
15. Jenkins, S. D. & Ruostekoski, J. Metamaterial transparency induced by cooperative electromagnetic interactions. *Phys. Rev. Lett.* **111**, 147401 (2013).
16. Bettles, R. J., Gardiner, S. A. & Adams, C. S. Enhanced optical cross section via collective coupling of atomic dipoles in a 2D array. *Phys. Rev. Lett.* **116**, 103602 (2016).
17. Facchinetti, G., Jenkins, S. D. & Ruostekoski, J. Storing light with subradiant correlations in arrays of atoms. *Phys. Rev. Lett.* **117**, 243601 (2016).
18. Facchinetti, G. & Ruostekoski, J. Interaction of light with planar lattices of atoms: reflection, transmission, and cooperative magnetometry. *Phys. Rev. A* **97**, 023833 (2018).
19. Shahmoon, E., Wild, D. S., Lukin, M. D. & Yelin, S. F. Cooperative resonances in light scattering from two-dimensional atomic arrays. *Phys. Rev. Lett.* **118**, 113601 (2017).
20. Fedotov, V. A. et al. Spectral collapse in ensembles of metamolecules. *Phys. Rev. Lett.* **104**, 223901 (2010).
21. Yang, Y., Kravchenko, I. I., Briggs, D. P. & Valentine, J. All-dielectric metasurface analogue of electromagnetically induced transparency. *Nat. Commun.* **5**, 5753 (2014).
22. Bettles, R. J., Gardiner, S. A. & Adams, C. S. Cooperative ordering in lattices of interacting two-level dipoles. *Phys. Rev. A* **92**, 063822 (2015).
23. Jenkins, S. D., Ruostekoski, J., Papasimakis, N., Savo, S. & Zheludev, N. I. Many-body subradiant excitations in metamaterial arrays: experiment and theory. *Phys. Rev. Lett.* **119**, 053901 (2017).
24. Plankensteiner, D., Sommer, C., Ritsch, H. & Genes, C. Cavity antiresonance spectroscopy of dipole coupled subradiant arrays. *Phys. Rev. Lett.* **119**, 093601 (2017).
25. Asenjo-Garcia, A., Moreno-Cardoner, M., Albrecht, A., Kimble, H. J. & Chang, D. E. Exponential improvement in photon storage fidelities using subradiance and selective radiance in atomic arrays. *Phys. Rev. X* **7**, 031024 (2017).
26. Jen, H. H. Phase-imprinted multiphoton subradiant states. *Phys. Rev. A* **96**, 023814 (2017).
27. Guimond, P.-O., Grankin, A., Vasilyev, D. V., Vermersch, B. & Zoller, P. Subradiant bell states in distant atomic arrays. *Phys. Rev. Lett.* **122**, 093601 (2019).
28. Hebenstreit, M., Kraus, B., Ostermann, L. & Ritsch, H. Subradiance via entanglement in atoms with several independent decay channels. *Phys. Rev. Lett.* **118**, 143602 (2017).
29. Grankin, A., Guimond, P. O., Vasilyev, D. V., Vermersch, B. & Zoller, P. Free-space photonic quantum link and chiral quantum optics. *Phys. Rev. A* **98**, 043825 (2018).
30. Olmos, B. et al. Long-range interacting many-body systems with alkaline-earth-metal atoms. *Phys. Rev. Lett.* **110**, 143602 (2013).
31. Krämer, S., Ostermann, L. & Ritsch, H. Optimized geometries for future generation optical lattice clocks. *Europhys. Lett.* **114**, 14003 (2016).

32. Yoo, S.-M. & Paik, S. M. Cooperative optical response of 2D dense lattices with strongly correlated dipoles. *Opt. Express* **24**, 2156 (2016).
33. Yoo, S.-M. Strongly coupled cold atoms in bilayer dense lattices. *N. J. Phys.* **20**, 083012 (2018).
34. Zeytinoğlu, S. & Imamoğlu, A. Interaction-induced photon blockade using an atomically thin mirror embedded in a microcavity. *Phys. Rev. A* **98**, 051801 (2018).
35. Mkhitaryan, V., Meng, L., Marini, A. & de Abajo, F. J. G. Lasing and amplification from two-dimensional atom arrays. *Phys. Rev. Lett.* **121**, 163602 (2018).
36. Lee, M. D., Jenkins, S. D. & Ruostekoski, J. Stochastic methods for light propagation and recurrent scattering in saturated and nonsaturated atomic ensembles. *Phys. Rev. A* **93**, 063803 (2016).
37. Thompson, R. J., Rempe, G. & Kimble, H. J. Observation of normal-mode splitting for an atom in an optical cavity. *Phys. Rev. Lett.* **68**, 1132–1135 (1992).
38. Khitrova, G., Gibbs, H. M., Kira, M., Koch, S. W. & Scherer, A. Vacuum Rabi splitting in semiconductors. *Nat. Phys.* **2**, 81–90 (2006).
39. Balik, S., Win, A. L., Havey, M. D., Sokolov, I. M. & Kupriyanov, D. V. Near-resonance light scattering from a high-density ultracold atomic ^{87}Rb gas. *Phys. Rev. A* **87**, 053817 (2013).
40. Chabé, J. et al. Coherent and incoherent multiple scattering. *Phys. Rev. A* **89**, 043833 (2014).
41. Pellegrino, J. et al. Observation of suppression of light scattering induced by dipole–dipole interactions in a cold-atom ensemble. *Phys. Rev. Lett.* **113**, 133602 (2014).
42. Sheremet, A. S. et al. Light scattering on the $F = 1 \rightarrow F' = 0$ transition in a cold and high density ^{87}Rb vapor. *J. Mod. Opt.* **61**, 77–84 (2014).
43. Kwong, C. C. et al. Cooperative emission of a coherent superflash of light. *Phys. Rev. Lett.* **113**, 223601 (2014).
44. Jennewein, S. et al. Coherent scattering of near-resonant light by a dense microscopic cold atomic cloud. *Phys. Rev. Lett.* **116**, 233601 (2016).
45. Kwong, C. C., Yang, T., Delande, D., Pierrat, R. & Wilkowski, D. Cooperative emission of a pulse train in an optically thick scattering medium. *Phys. Rev. Lett.* **115**, 223601 (2015).
46. Bromley, S. L. et al. Collective atomic scattering and motional effects in a dense coherent medium. *Nat. Commun.* **7**, 11039 (2016).
47. Jenkins, S. D. et al. Optical resonance shifts in the fluorescence of thermal and cold atomic gases. *Phys. Rev. Lett.* **116**, 183601 (2016).
48. Guerin, W., Araújo, M. O. & Kaiser, R. Subradiance in a large cloud of cold atoms. *Phys. Rev. Lett.* **116**, 083601 (2016).
49. Corman, L. et al. Transmission of near-resonant light through a dense slab of cold atoms. *Phys. Rev. A* **96**, 053629 (2017).
50. Machluf, S., Naber, J. B., Soudijn, M. L., Ruostekoski, J. & Spreeuw, R. J. C. Collective suppression of optical hyperfine pumping in dense clouds of atoms in microtraps. *Phys. Rev. A* **100**, 051801 (2019).
51. Ruostekoski, J. & Javanainen, J. Quantum field theory of cooperative atom response: low light intensity. *Phys. Rev. A* **55**, 513–526 (1997).
52. Morice, O., Castin, Y. & Dalibard, J. Refractive index of a dilute bose gas. *Phys. Rev. A* **51**, 3896–3901 (1995).
53. Skipetrov, S. E. & Sokolov, I. M. Absence of Anderson localization of light in a random ensemble of point scatterers. *Phys. Rev. Lett.* **112**, 023905 (2014).
54. Sperling, T. et al. Can 3D light localization be reached in 'white paint'? *N. J. Phys.* **18**, 013039 (2016).
55. Javanainen, J., Ruostekoski, J., Vestergaard, B. & Francis, M. R. One-dimensional modeling of light propagation in dense and degenerate samples. *Phys. Rev. A* **59**, 649–666 (1999).
56. Jones, R., Saint, R. & Olmos, B. Far-field resonance fluorescence from a dipole-interacting laser-driven cold atomic gas. *J. Phys. B* **50**, 014004 (2017).
57. Lee, M. D., Jenkins, S. D., Bronstein, Y. & Ruostekoski, J. Stochastic electrodynamics simulations for collective atom response in optical cavities. *Phys. Rev. A* **96**, 023855 (2017).
58. Krämer, S. & Ritsch, H. Generalized mean-field approach to simulate the dynamics of large open spin ensembles with long range interactions. *Eur. Phys. J. D* **69**, 282 (2015).
59. Sutherland, R. T. & Robicheaux, F. Degenerate zeeman ground states in the single-excitation regime. *Phys. Rev. A* **96**, 053840 (2017).
60. Zhang, Y.-X. & Mølmer, K. Theory of subradiant states of a one-dimensional two-level atom chain. *Phys. Rev. Lett.* **122**, 203605 (2019).
61. Henriet, L., Douglas, J. S., Chang, D. E. & Albrecht, A. Critical open-system dynamics in a one-dimensional optical-lattice clock. *Phys. Rev. A* **99**, 023802 (2019).
62. Parmee, C. D. & Cooper, N. R. Phases of driven two-level systems with nonlocal dissipation. *Phys. Rev. A* **97**, 053616 (2018).
63. Gross, C. & Bloch, I. Quantum simulations with ultracold atoms in optical lattices. *Science* **357**, 995–1001 (2017).
64. Nogrette, F. et al. Single-atom trapping in holographic 2D arrays of microtraps with arbitrary geometries. *Phys. Rev. X* **4**, 021034 (2014).
65. Bernien, H. et al. Probing many-body dynamics on a 51-atom quantum simulator. *Nature* **551**, 579–584 (2017).
66. Meystre, P. & Sargent III, M. *Elements of Quantum Optics* (Springer, Berlin, Heidelberg, 2007).
67. Wootters, W. K. Entanglement of formation of an arbitrary state of two qubits. *Phys. Rev. Lett.* **80**, 2245–2248 (1998).
68. Adamo, G. et al. Electron-beam-driven collective-mode metamaterial light source. *Phys. Rev. Lett.* **109**, 2174 (2012).
69. Rui, J. et al. A subradiant optical mirror formed by a single structured atomic layer. *Nature* **583**, 369–374 (2020).
70. Keaveney, J. et al. Cooperative Lamb shift in an atomic vapor layer of nanometer thickness. *Phys. Rev. Lett.* **108**, 173601 (2012).

Acknowledgements

Author contributions
R.J.B. performed the numerical simulations with assistance from M.D.L. J.R. and R.J.B. developed the theory and derivations. R.J.B., S.A.G., and J.R. contributed to the manuscript text and R.J.B. generated the figures.

Competing interests
The authors declare no competing interests.

Additional information